LES of the aero-acoustic coupling in acoustic liners containing multiple cavities

Michaël Bauerheim, Laurent Joly

LES of the aero-acoustic coupling in acoustic liners containing multiple cavities

M. Bauerheim* and L. Joly†
ISAE-Supaéro, Toulouse, 31400, France

Acoustic liners are specific devices dedicated to reduce noise pollution of aircraft. They contained a large number of cavities which are submitted to a turbulent grazing boundary flow. In some cases, the shear layer can become unstable, and couples with the acoustic waves propagating in the cavity, leading to a strong vortex-noise interaction. Whereas this vortex-noise coupling is well known in single-cavity configurations where the boundary layer can be described by its upstream characteristics, the interaction between a turbulent grazing flow and multiple cavities is less understood, mainly because the boundary layer may evolve along the liner. This study investigates numerically the coupling between acoustic waves and hydrodynamic fluctuations in an academic liner configuration containing multiple deep cavities. First a single 3D cavity is simulated using LES, revealing a strong vortex-noise coupling at the frequency of the quarter-wave mode at 750Hz, due to a shear layer instability with a wavelength shorter than the cavity width. Then, both a 2D and 3D configuration containing 101 cavities are computed and analyzed. When the acoustic feedback loop is cut off, no vortex-noise coupling occurs, however large flow structures can be observed in the boundary layer. When switching on the acoustic feedback loop, the vortex-noise coupling at 750Hz is again present, yet a more complex noise spectrum is obtained. In particular, lower frequencies are observed, associated to intermittency due to the desynchronization between cavities. Moreover, it is shown that the boundary layer evolves along the liner. One key phenomenon is the massive instability of the turbulent boundary layer, generating large coherent structures with a wavelength larger than the cavity width in the downstream part of the liner. A scenario is then proposed to explain this competition between these two phenomena: in the upstream part of the liner, the flow is dominated by the vortex-noise coupling at $750Hz$. Further downstream, however, the shear layer becomes thicker, and is therefore more robust to transverse acoustic excitation, leaving the place for the large turbulent flow structures in the boundary layer to dominate the flow field.

I. Introduction

Acoustic liners are devices widely employed to mitigate noise pollution emitted from transport vehicles, as for example in the air intake of aeronautical engines or in air conditioning systems. They usually consist in one (SDOF) or two (DDOF) layers containing multiple cavities (e.g. honeycomb structure) combined with a perforated porous face-sheet. In most engineering applications, a flow is present along the liner, which therefore leads to an interaction between the external boundary layer and the acoustic liner. For a single cavity, a constructive interference can occur when the standing acoustic mode in the cavity couples with the hydrodynamic instability of the shear layer acting as an acoustic dipolar source term. This phenomenon has been intensively investigated experimentally [1–6], numerically [7–9] and theoretically [4, 10, 11]. Whereas this interaction is well understood for a single cavity interacting with a grazing flow, it is less studied for configurations containing multiple close cavities. Surprisingly, under peculiar circumstances, sound waves might be amplified by the damping device rather than attenuated. This occurs when hydrodynamic instabilities are triggered by the low-resistance liner. Early experiments conducted by Meyer and Kurtze [12], Brandes and Ronneberger [13] and later by Juschke [14] have revealed that amplification arises in an array of thin-walled cavities for excitation frequencies close to the resonance frequency of the liner. It suggests that, as for single-cavity cases, a constructive coupling between the hydrodynamic instability and the standing acoustic mode in the cavity is generating a vortex-induced noise. In similar configurations, Marx et al. [15] have carried out PIV and LDV revealing the presence of spanwise coherent flow structures inside the boundary layer. Recently, stability analysis have

*Associate Professor, ISAE-Supaéro DAEP, michael.bauerheim@isae-supaero.fr
†Professor, ISAE-Supaéro DAEP, laurent.joly@isae-supaero.fr

been performed [16–18], demonstrating that these large structures are induced by a convective instability due to the periodicity of the liner, as a consequence of the Floquet-Bloch theorem [18]. The amplification of this Bloch unstable mode appears in a limited range of frequencies, close and slightly above the quarter-wave mode of the cavity. In most of these studies however, a major difficulty lies in the definition of the relevant baseline flow, since the boundary layer flow experiences a fast evolution along the liner because of the unstable Bloch mode. for instance, the mean flow is usually assumed unaltered over the the liner. An other assumption is the cavity-by-cavity approach, which suggests that all cavities respond in the same manner to the flow disturbances. These assumptions have been relaxed by the use of a more relevant baseline flow, extracted from an experiment of a simulation, coupled with Linearized Navier-Stokes Equations (LNSE) computations for the perturbations. For a single cavity configuration, Boujo et al. [9] have shown that such an approach is able to reproduce correctly both the linear and non-linear response of the unstable shear layer to the incoming acoustic waves. For liner cases, Xin et al. [19] have obtained the sound transmission coefficients and the velocity fluctuations in a lined duct similar to [15] using LNSE and an experimental baseline flow. Accounting for the spatial evolution of the flow over the liner has lead to a good agreement for the transmission coefficient compared with experimental measurements, yet near-wall fluctuating velocity fluctuations were still significantly under-predicted. Similarly, Burak et al. [20] have obtained an instability pattern combining both LNSE and a base flow computed by RANS. To reduce the computational time, most of these studies employs an equivalent Impedance Boundary Condition (IBC) as a surrogate model of the complete liner geometry. The IBC $Z_(\omega)$ is defined, either in the frequency- or time-domaine, by

$$\hat{Z}(\omega) = \frac{\hat{p}(\omega)}{\rho_0 c_0 \hat{v}(\omega)} \tag{1}$$

where $\hat{Z}(\omega)$ is the dimensionless acoustic impedance, $\hat{p}$ is the complex acoustic pressure and $\hat{v}$ is the complex wall-normal velocity fluctuation. ρ_0 and c_0 are the mean density and sound speed.

Most numerical simulations solving the Navier-Stokes equations for acoustic liners, thus accounting for multiple cavities, rely on imposing an equivalent IBC as a surrogate model for the whole device. The main advantage is to reduce the computational cost since the flow and acoustic inside the cavities are not actually solved. Note that imposing an impedance, usually defined and measured in the frequency domaine, in a time-marching CFD solver is not straightforward. The classical NSCBC approach [21] can be used to apply the reflection coefficient $\hat{R} = \frac{1-\hat{Z}}{1+\hat{Z}}$, at least in a limited range of frequency. However, imposing a non-null phase $\angle Z$ requires advanced computational methods, such as the Time-Domain Impedance Boundary Condition of Tam and Auriault [22]. For instance, Burak et al. [20] solved the Navier-Stokes equations with slip-walls and the TD-IBC [22]. Recently, Large Eddy Simulations (LES) of a fully developed turbulent channel flow have been realized [23] with an IBC applied on one wall. Interestingly, they evidence that a low-resistance, typically $\Re(\hat{Z}) = 0.01$, can trigger hydrodynamic instabilities without external acoustic forcing. Similarly, Bodart et al. [24] have performed LES of a turbulent separation control via the IBC on a NACA 4412 airfoil in near-stalled conditions. They show again that a low-resistance IBC is able to modify the boundary layer evolution along the suction side leading to a delay in the boundary layer separation accompanied with a higher lift coefficient.

While existing studies have already demonstrated that hydrodynamic instabilities can developed over liner, the physical mechanisms of this phenomenon remains unclear. To further understand the vortex-noise coupling in multiple-cavity configurations, one may incorporate the cavities within the computational domain to (i) obtain time-resolved data near the orifices, especially on the turbulent boundary layer development along the liner, and (ii) on the acoustic waves inside the cavity, in particular to revealed the correlation between cavities. Where as simulations of a turbulent grazing flow over a cavity has already been realized [7, 25], LES of turbulent 3D configurations containing numerous cavities are still rare because highly CPU demanding. One example has been conducted recently by Shelekhov et al. [26] where 77 cavities have been simulated in 2D with very deep cavities. In this paper, both a single-cavity and multiple-cavity configurations will be computed using LES on 2D and 3D domains. The acoustic liner geometry consists in simple deep cavities with aspect ratio $H/W = 3$ at a low Mach number. For the liner configurations, 101 2D and 3D cavities have been incorporated into the computational domain. The detailed numerical setup and the liner geometry are described in Section II. Results on the 3D single-cavity case (Section III.A) as well as the 2D and 3D results on the liner containing 101 cavities (Section III.B) are provided in Section III, where both the turbulent boundary layer flow and the acoustic waves inside the cavity are analyzed. It shows that the hydro-acoustic interaction with successive cavities can trigger complex hydrodynamic perturbations in the boundary layer, especially low-frequency modes. Moreover, along the liner, both the nature and characteristics of the boundary layer evolve, and therefore affect back the oscillations in the limit cycle observed inside the cavity. Finally, it is shown that this effect depends strongly on the dimensionality of the problem: for a 2D problem, both the hydrodynamic perturbations and the acoustic oscillations are reduced along the liner, whereas for a 3D case, the amplitude of the oscillations slightly increase along the liner.

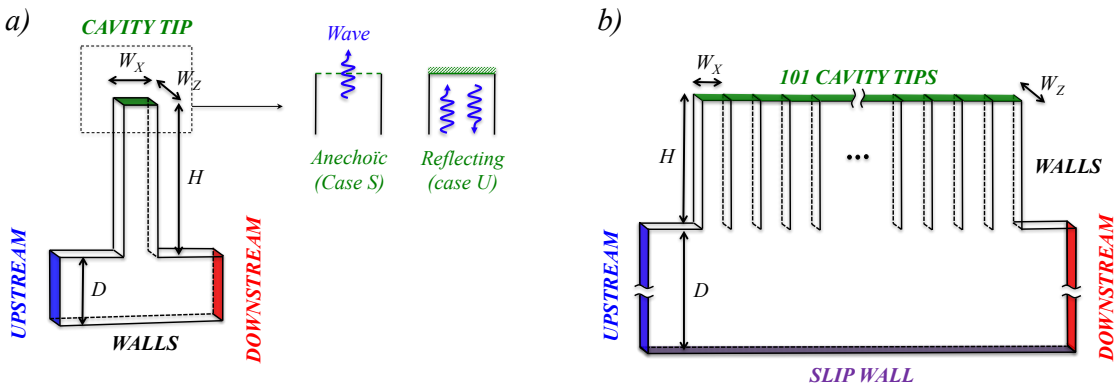

Fig. 1 The single (left, a), and multiple (right, b) configurations investigated. For both cases, the tip boundary condition can be switched from anechoic to reflecting.

II. Numerical setup

To investigate the turbulent boundary layer interaction with the acoustic liner, 3 configurations are retained. First, the classical 3D T-junction computed in Boujo et al. [9] is considered (Fig. 1-a), called case *C1_3D*. It contains a deep cavity of aspect ratio $W/H = 1/3$, connected to a main pipe. At the junction, the typical cell size is $300\mu m$, leading to $y^+ < 5$ at walls. Walls are therefore treated as no-slip and adiabatic. The Vreman model [27] is adopted to account for the small turbulent scales. A turbulent mean velocity profile is injected at the inlet, characterized by a bulk velocity $U_b = 56m/s$ and a power-law profile where the exponent is set to $1/7$. Note however that no synthetic turbulence is injected at the inlet. The associated Reynolds number is $R_e = U_b W/\nu \approx 1.5\ 10^5$, where $\nu = 1.12\ 10^{-5} m^2 s^{-1}$ is the kinematic viscosity of the air. Knowing that the width-to-depth ratio of the side cavity is $W_X/L_T = 1/3$, interactions between the shear layer instability and the quarter-wave mode of the side tube are expected [28]. The mesh is a multi-block structured grid composed of 1.2 millions hexa. The maximum cell size is $\delta x = 1mm$ which allows acoustic waves to be resolved on the grid (10 points per wavelength) for frequencies up to $f_{max} = c_0/N\delta x = 34\ kHz$. For hydrodynamic modes which are convected at a lower speed, typically $0.4U_b$ in the vortex sheet characterized by $\delta x = 0.3mm$, the maximal resolved frequency is $f_{max} = 0.4U_b/N\delta x = 7466Hz$. The transverse direction is discretized with 30 cells which represents $W_Z/W_X = 33\%$ of the cavity width, and periodic conditions are applied. The upstream/downstream non-reflecting boundary conditions are imposed using the NSCBC formalism developed by Poinsot and Lele [21]. They are located far from the cavity junction to limit their effect, typically $5W_X$ upstream and $9W_X$ downstream. For the outlet condition, an additional sponge zone is defined where the numerical scheme is switched to first order, in order to dissipate flow structures and thus limiting spurious acoustic wave reflections at this boundary. The boundary at the tube tip (Fig. 1-a) can be set as non-reflecting to obtain a stable simulation (case *C1_3D_S*). From this case, the tube tip boundary condition is then imposed as perfectly reflecting, i.e. a classical no-slip wall, to investigate potential unstable modes (case *C1_3D_U*). As shown in Section III, an unstable mode at $750Hz$ grows exponentially in time until a limit cycle governed by a non-linear saturation [9]. Since the only difference between case *C1_3D_S* and *C1_3D_U* is the acoustic treatment of the side tube, it ensures that the unstable mode is controlled by the vortex-sound coupling in the side branch.

Then, a configuration containing $N_c = 101$ 2D cavities is simulated, called case *C101_2D_U* (Fig. 1-b). The same geometry and mesh characteristics are considered, however no turbulence model is employed here because of the 2D flow topology, and the main channel is now semi-open with a ratio $D/W_X = 35$ as shown in Fig. 1. Moreover, a sponge layer is applied at the bottom wall, and a non-reflecting NSCBC condition is applied. The resulting mesh contains 3.6 millions quads. This configuration allows the computation of the vortex-noise coupling for long time, since the 2D simulation is affordable. Results will be compared qualitatively with the simulations of Shelekhov et al. [26] on a similar 2D case containing 77 cavities. Finally, a 3D version of the multiple-cavity case will be computed. The same mesh characteristics are employed, leading to a structured mesh containing 73.5 millions cells. Compared with the single-cavity case, the transverse direction is limited to $W_Z/W_X = 20\%$ of the cavity width, and discretized on 20 points, to reduce the computational time. As for the single-cavity configuration, the tip boundary condition will be switched from non-reflecting (case *C101_3D_S*) to reflecting (case *C101_3D_U*), to ensure that the hydrodynamic

instabilities observed are associated with a vortex-noise coupling due to the acoustic liner. The several configurations are summarized in Tab. 1.

Name	2D/3D	N_c	BC tip	BC bottom	$H(mm)$	$D(mm)$	W_X/H	W_Z/W_X	N_{cells} (10^6)
C1_3D_S	3D	1	Non-Refl.	No-Slip	90	62	1/3	33%	1.2
C1_3D_U	3D	1	Refl.	No-Slip	90	62	1/3	33%	1.2
C101_2D_U	2D	101	Refl.	Slip	90	1062	1/3	–	3.6
C101_3D_S	3D	101	Non-Refl.	Slip	90	1062	1/3	20%	73.5
C101_3D_U	3D	101	Refl.	Slip	90	1062	1/3	20%	73.5

Table 1 Configurations investigated in this paper, where N_c is the number cavities and N_{cells} the number of cells in the mesh.

In this study, the T-junction and the acoustic liners are investigated thanks to Large Eddy Simulation (LES). LES are performed using the massively parallel finite-volume code Charles^X. It solves the filtered 2D and 3D compressible Navier-Stokes equations on unstructured meshes, yet here a structured mesh has been employed. This solver has already been applied to a large variety of problems, raning from shock-turbulence boundary layer interaction, to high-Reynolds number flows [24, 29]. The grid spacing is constant in the whole boundary layer as well as close to the cavity orifice. Charles^X employs a variable-stage Runge- Kutta time discretization and a grid-adaptive reconstruction strategy, blending a high-order polynomial interpolation with low-order upwind fluxes [30]. The code is parallelized using the Message Passing Interface (MPI) protocol and is highly scalable on a large number of processors [31]. In the present study, the LES solver was run on the ISAE-Supaero's supercomputer Pando, up to 384 processors for cases *C101_3D_S* and *C101_3D_U*.

III. Results

A. Single cavity whistling

First, the tip boundary condition is set to non-reflecting to ensure the non-reflection of acoustic waves and therefore removing the acoustic feedback loop in the system. In such a case, the system is stable (Case *C1_3D_S*, `---` in figure 2), where only small pressure fluctuations around $1200Hz$ are observed, with typical amplitudes of $20Pa$. The Strouhal number is $S_t = fW_X/U_b = 0.53$, typical of Strouhal numbers where the second hydrodynamic mode is dominant (range $[0.5,\ 0.7]$), as shown in Boujo et al. [9] on the same configuration. This case is therefore considered as stable.

Based on case *C1_3D_S*, the boundary condition is now switched to non-reflecting (case *C1_3D_U*). A strong coupling occurs, leading to pressure oscillations at $750Hz$ and amplitude $\pm 250\ Pa$ in the limit cycle. This results is validated using the simulation of Boujo et al. [9] on the same case with another LES 3D compressible code, called AVBP. From the PSD, both frequencies and amplitudes of the fundamental modes and its harmonics are well reproduced between the two codes. These oscillations correspond to a self-excited mode where the frequency is associated with the quarter-wave mode of the tube. The Strouhal number is $S_t = 0.40$, typical of instabilities involving the first hydrodynamic mode. The higher harmonics are also present with a lower amplitude. The difference between the two present cases indicates that the acoustic mode is unstable, potentially driven by the vorticity production at the junction. The limite cycle is perturbed by the other harmonics as well as turbulence. The main scenario retained for the instability is that the shear layer becoming unstable, high vorticity is produced at the junction cavity. It yields an unsteady Coriolis force f_c', which can be written $\vec{f_c'} = -\rho\vec{\omega}' \times \vec{U}$, where $\vec{\omega}'$ is the unsteady vorticity, and $\vec{U}$ is the time-averaged velocity field. As an unsteady force, it is a dipolar source term for acoustics. Acoustic waves will therefore propagate inside the cavity, before being reflected back due to the no-slip wall boundary condition at the tip of the cavity. This new wave propagates towards the shear layer, creating an external forcing at the frequency of the acoustic waves, which can further destabilize the system in some conditions. This closed loop system becomes stable when the acoustic feedback loop is turned off. When unstable, the oscillations grow exponentially in the linear regime before reaching a plateau controlled by non-linearities where the source term balances acoustic losses. More details on these mechanisms in the present single-cavity configuration can be found in Boujo et al. [9] as well as in the companion paper [32].

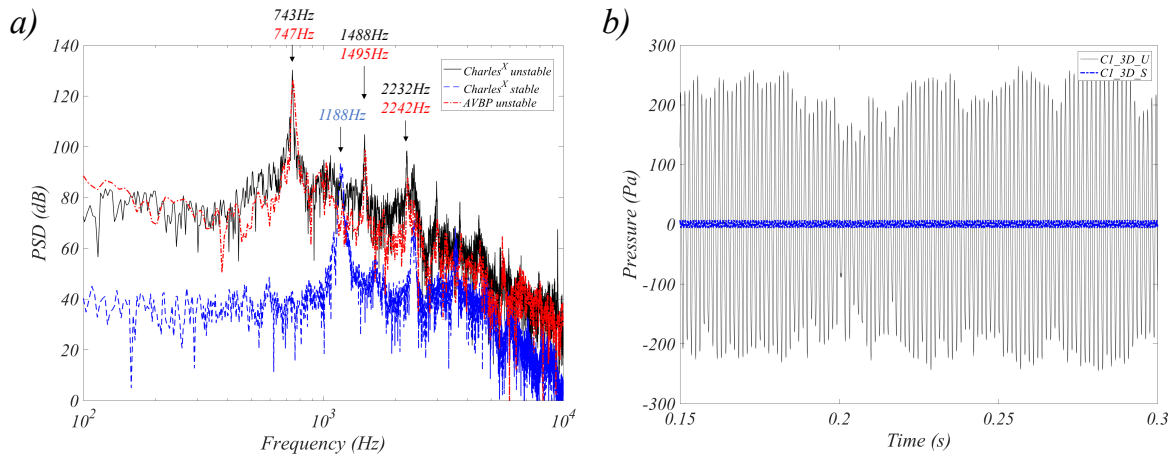

Fig. 2 a) Power spectral density of the pressure fluctuations at the tip cavity, normalized by the reference pressure $20\mu Pa$, for three configurations: *C1_3D_U* (——), *C1_3D_S* (- - -), and *C1_3D_U* (-·-·-) computed by another LES code (AVBP). b)Temporal evolution of the pressure at the cavity tip for both the stable unstable cases.

B. 2D and 3D acoustic liners

In order to investigate the vortex-noise coupling in an acoustic liner containing multiple cavities, $N_c = 101$ cavities have been simulated in both 2D and 3D (Tab. 1). The geometry and inlet flow are the same than for the single-cavity case studied in Section III.A except for the much larger height D of the main channel to avoid large turbulent structures to interact with the bottom wall, as well as the transverse direction W_Z which has been reduced to save computational time. For the results, the transient part has been discarded before collecting statistics.

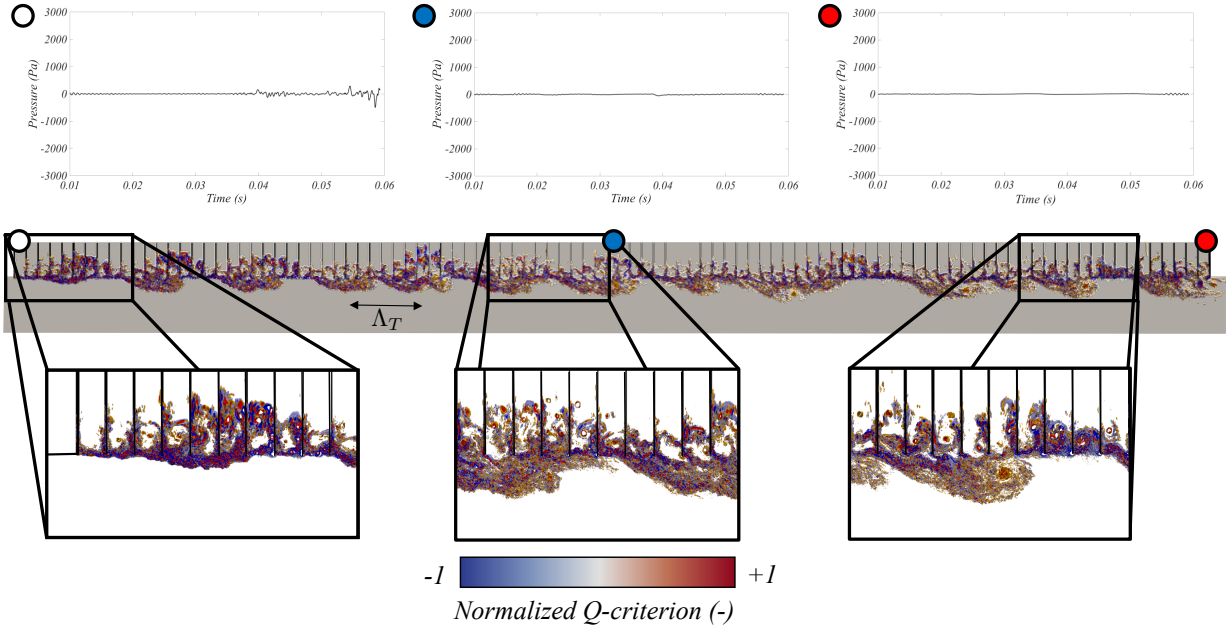

Fig. 3 Instantaneous snapshot (middle) of the Q-criterion for case *C101_3D_S*, highlighted by zooms (bottom) to indicate the evolution of the 3D boundary layer along the liner. The temporal evolution of the fluctuating pressure at 3 cavity tips (cavity n°1, n°51 and n°101) are also displayed (top).

1. Acoustic liner with non-reflecting boundary conditions (open-loop system)

First, the simulation of the 3D configuration containing 101 cavities has been simulated by applying a non-reflecting NSCBC boundary condition at all tips of the cavities (*C101_3D_S* in Tab. 1). Such a treatment avoids the acoustic waves to be reflected back to the shear layer, thus preventing the vortex-noise coupling: in other words, it is equivalent to an open-loop system with a liner containing infinitely-long cavities. The same case in 2D has been simulated, but not shown here since conclusions are equivalent to the 3D case. More quantitative details on the acoustic and turbulent fluctuations in 2D, compared with 3D, will be given for the unstable case in Section III.B.2. Figure 3 displays the instantaneous Q-criterion for the case *C101_3D_S*, as well as the pressure fluctuations at the tip of three cavities: the cavity $n^\circ 1$ (first cavity at the upstream edge), $n^\circ 51$ (middle of the liner) and $n^\circ 101$ (last cavity at the downstream edge). As expected, no acoustic pressure fluctuations are observed at the cavity tips, since the acoustic feedback loop as been opened: no acoustic resonance in the cavities can occur. The small pressure fluctuations observed are therefore due to the direct noise generated by the grazing turbulent boundary layer, going out of the computational domain since non-reflecting BCs are applied.

Surprisingly, even if the aero-acoustic system is stable, large turbulent structures are developing along the liner, as depicted by the Q-criterion in Fig. 3. These structures were not observed in the single-cavity configuration, yet they emerge very rapidly, after the third cavity. The amplitude of these large hydrodynamic perturbations increases while being convected downstream, with a roll-up appearing after a dozen of cavities. Its associated wavelength is approximately $\Lambda_T \approx 8W_X$ (12 to 13 structures are seen over 101 cavities of width W_X). Above these structures, an intense vortical flow is generated inside the cavities. Note that this case has been initialized in two different ways: (i) using the mean inlet profile everywhere, and (ii) using the unstable case *C101_3D_U*, and switching the boundary of cavities' tip to non-reflecting. Similar results were obtained for both initializations, ensuring that the physics and the present conclusions are not dependent on initial perturbations. Consequently, this case is exhibiting a similar behavior than the 2D simulations performed by Shelekhov et al. [26] for $N_c = 77$ with very deep cavities (their aspect ratio H/W_x was varied from 20 to 80, whereas here $H/W_x = 3$). In particular, they obtained large turbulent flow structures combined with intense vortical flows inside cavities, whatever this aspect ratio. It suggests that this phenomenon (i) requires the presence of multiple cavities, since not observed in cases *C1_3D_S* and *C1_3D_U*, (ii) is not directly triggered by transverse acoustic waves, but (iii) once triggered, might be affected by acoustics inside the cavities (otherwise all results from Shelekhov et al. [26]would have been identical if not depend on transverse acoustics, characterized by the ratio H/W_X.)

2. Acoustic liner with reflecting boundary conditions (closed-loop system)

In the previous section, large flow structures have been observed in the boundary layer when the transverse acoustic feedback loop has been cut off. In this section, the closed-loop system is now investigated by using reflecting boundary conditions at each cavity's tip. Other parameters are unchanged. Figures 4 and 5 display an instantaneous snapshot of the z-component of the vorticity field for the two unstable cases *C101_2D_U* and *C101_3D_U*.

In both case, it reveals that the initial thin boundary layer evolves along the liner: a thicker boundary layer is obtained upstream. Moreover, large coherent structures in the flow are noticed, even in presence of the 3D turbulence in case *C101_3D_U*. In 2D, the velocity fluctuations are only coherent vortices of various scales, where the largest scale observed is the order of magnitude of the cavity width W_X. The flow is therefore composed of condensat, where small vorticies can aggregate because of vortex pairing. However on the 3D case, the largest structures are composed of thin flow structured rolled-up and growing while being convected downstream. The largest size observed is around 4 times the cavity width. The spatial distance between these structures are denoted Λ_T, and varied along the liner. For the first cavities, $\Lambda_T \approx W_X$ (as in a single-cavity congiguration), whereas further downstream $\Lambda_T \approx 5W_X - 8W_X$ (as in the previous multiple configuration *C101_3D_S*). This large structures are similar to ones observed by Dai and Aurégan [18] in their stability analysis of a a liner containing 30 cavities. Note that since no synthetic turbulence is injected in the case *C101_3D_U*, the first cavities experience only a coherent rolled-up of the shear layer. After a few cavities, the successive interactions of the shear layer with the cavity edge leads to a large vorticity production, either coherent vorticies in the 2D case, or turbulence in the 3D case. Thus, the unsteady behavior of the shear layer is evolving along the liner, which is one of the major differences compared with the previous stable case, for which the characteristics of these flow structures remained constant along the liner. Note also that now, large acoustic fluctuations occur at the cavity's tip, in both 2D and 3D, revealing the presence of a vortex-noise coupling. In particular, it suggests here a competition between (i) the vortex-noise coupling leading to the unstable mode involving the transverse acoustic waves inside the cavities, as in the single cavity case *C1_3D_U*, and (ii) the boundary layer instability with large flow structures

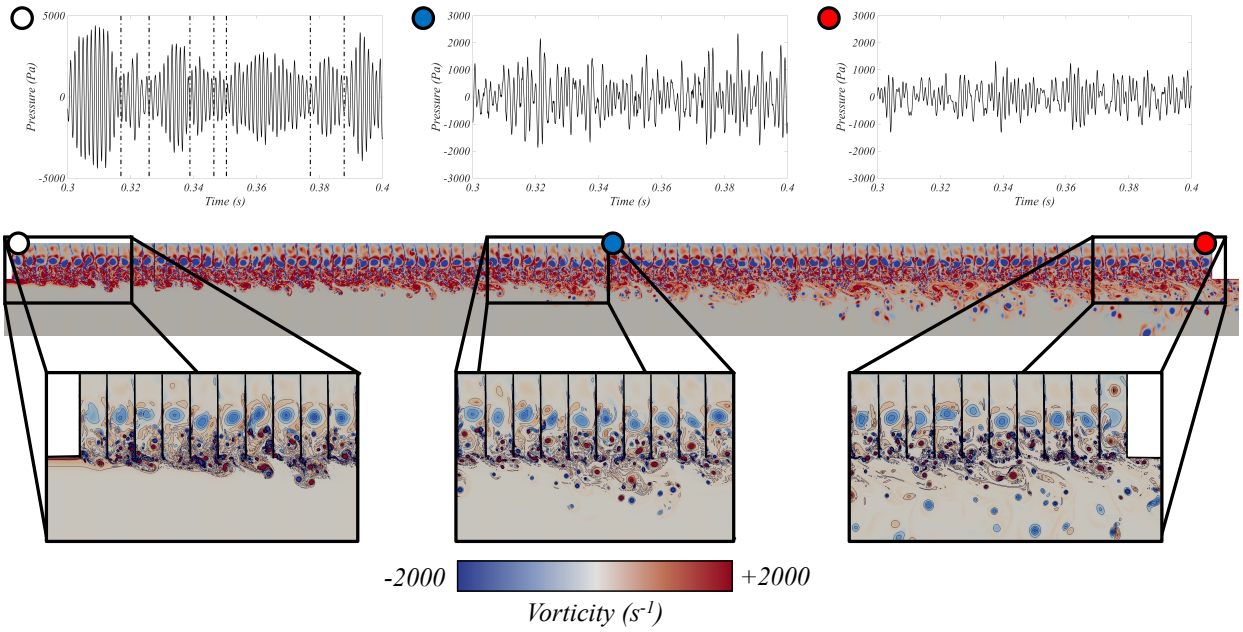

Fig. 4 Instantaneous snapshot (middle) of the z-component of the 2D vorticity field for case *C101_2D_U*, highlighted by zooms (bottom) to indicate the evolution of the 2D boundary layer along the liner. The temporal evolution of the fluctuating pressure at 3 cavity tips (cavity n°1, n°51 and n°101) are also displayed (top).

convected downstream, as in the multiple stable case *C101_3D_S*.

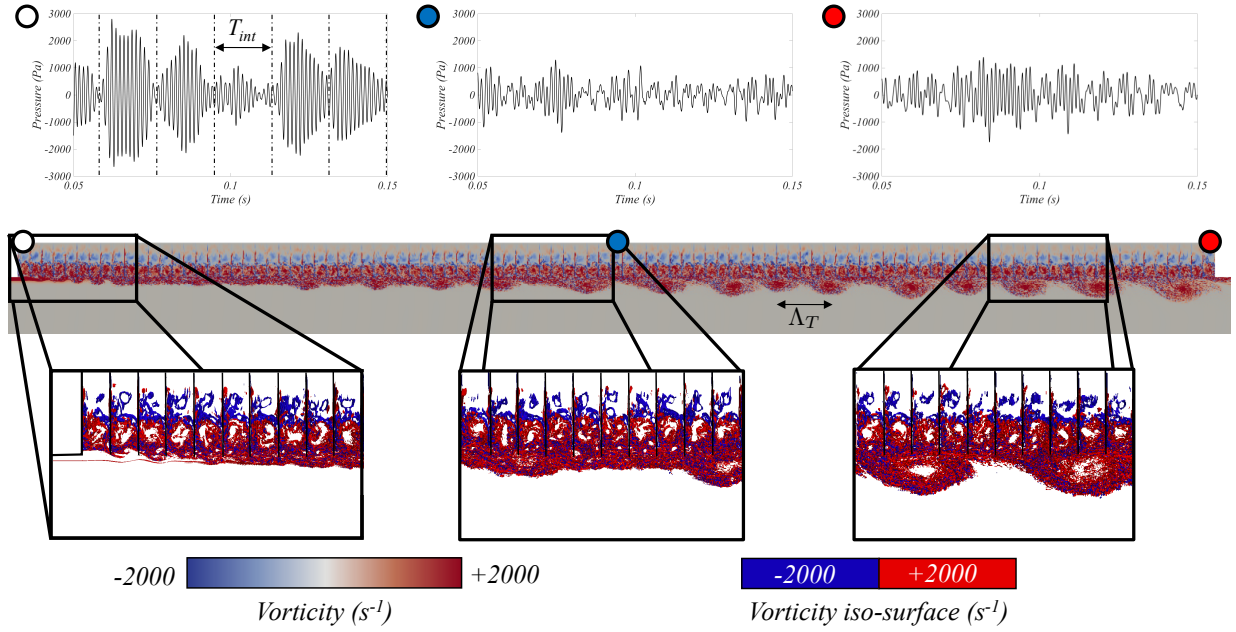

Fig. 5 Instantaneous snapshot (middle) of the z-component of the 3D vorticity field for case *C101_3D_U*, highlighted by zooms (bottom) to indicate the evolution of the 3D boundary layer along the liner. The temporal evolution of the fluctuating pressure at 3 cavity tips (cavity n°1, n°51 and n°101) are also displayed (top).

Such an evolution along the liner is further detailed in Fig. 6. Indeed, most studies investigating acoustic liners with

multiple cavities assume that the boundary layer does not evolve in the spanwise direction. Thus, the mean axial velocity profiles at several locations are provided, showing that the boundary layer profile evolves from the $1/7$ power-law at the upstream cavity towards a more complex profile at the downstream part of the liner. One of the key phenomenon is a thickening of the shear layer. This may be quantified by the boundary layer thickness δ^*/H and θ/H:

$$\delta^*/H = \int_{-\infty}^{0} \left(1 - \frac{U_X(y/H)}{U_E}\right) d\left(\frac{y}{H}\right) \tag{2}$$

$$\theta/H = \int_{-\infty}^{0} \frac{U_X(y/H)}{U_E}\left(1 - \frac{U_X(y/H)}{U_E}\right) d\left(\frac{y}{H}\right) \tag{3}$$

where U_E is the external axial velocity, obtained as the maximum axial velocity in the profile.

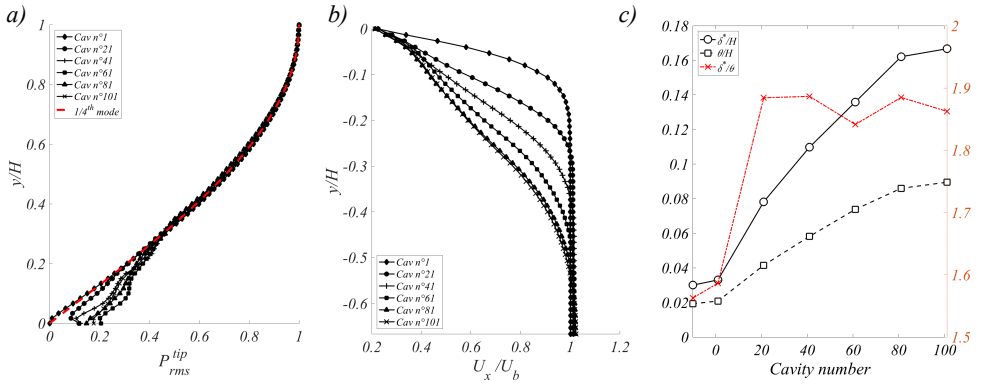

Fig. 6 Mean axial velocity profile U_X/U_b (left), rms value of the pressure at the cavity tip (middle), and evolution of the boundary layer thickness δ^*/H, θ/H and the shape factor δ^*/θ (right) for the case *C101_3D_U*.

These two boundary layer thickness are plotted in Fig. 6, showing a strong thickening of the shear layer along the liner. In particular, it is known that the shear layer thickness is one of the main parameters controlling the hydrodynamic instability: a thicker shear layer being usually more stable. This is one explanation for the reduced amplitude oscillations observed for downstream cavities: since the shear layer is thicker, the shear layer is less unstable leading to a reduced vortex-driven acoustic source term, thus limiting the acoustic resonance in the cavity. When this instability is reduced downstream, the large flow structures can now dominate: this scenario would explain the competition between these two phenomena, leading to the evolution of both acoustic and hydrodynamic characteristics along the liner. Finally, it is also shown that the axial velocity profile starts to converge towards a fixed profile for cavitis after $Nc > 80$, which suggests long acoustic liner should be investigated to extract the whole behavior of the hydrodynamic-acoustic coupling and competition. This can be also observed from the shear layer thickness δ^*/H and θ/H, which are still increasing after 80 cavities. Yet, one can notice that the shape factor δ^*/θ remains almost constant for cavities $N_c > 20$, which suggests that the nature of the boundary layer is however determined rapidly. In other words:

- $1 < N_c < 20$: the boundary layer nature is evolving because of the turbulence generation due to the successive interations with the cavities. Meanwhile, the boundary layer is also being thickened.
- $N_c > 20$: the nature of the boundary layer is now fully determined (i.e. turbulent), and only the shear layer is just thickened.

In Figs. 4 and 5, the temporal evolution of the pressure fluctuations at the cavity tip for three locations (marked by ∘), corresponding to the cavity n°1, n°51 and n°51, are also displayed. First, in both cases, a strong coupling occurs since high pressure levels are obtained in the cavity. To demonstrate that the nature of these oscillations are due to the interactions of the boundary layer with the acoustic waves inside the cavities, the boundary conditions at the cavities tip have been switched to non-reflecting, thus cutting out the acoustic feedback loop. The results of case *C101_3D_S* (Fig. 3) prove that no pressure fluctuations are observed: the amplitude of the oscillations is less than $100Pa$ for most cavities. Thus, the same vortex-noise coupling than in the single-cavity configuration occurs. However, while for a single cavity, the amplitude of oscillations at the limit cycle was $250Pa$, here it strongly depends on the cavity location. For instance, the first cavity experiences a much larger pressure oscillations (around $5000Pa$ in *C101_2D_U*, and $3000Pa$ in *C101_3D_U*), whereas the maximum amplitude of the oscillations in the last cavity is approximately $1000Pa$

in both 2D and 3D. It therefore shows that there is a cumulative effect due to the acoustic waves emitted from the other cavities: in particular for the first cavity, the acoustic level is almost 10 times the ones observed in the single-cavity case.

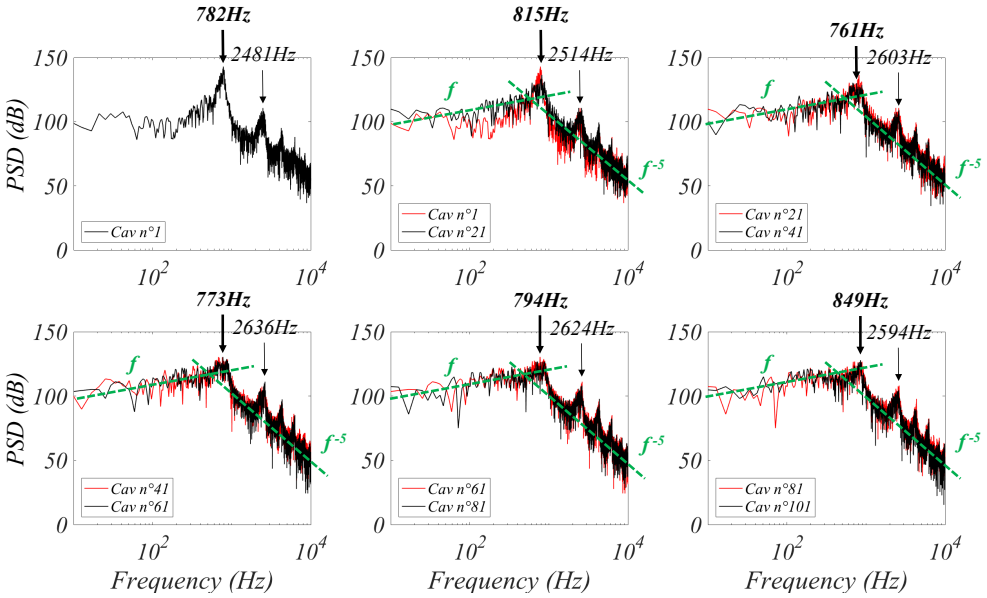

Fig. 7 Power spectral density (PSD) of the fluctuating pressure at six cavity tips (n°1, n°21, n°41, n°61, n°81 and n°101) for the case *C101_2D_U*. The evolution of the spectrum along the liner is highlighted by superimposition of the current spectrum (black) with the previous one (red).

Note also that for all cavities, the pressure oscillations have not a steady limit cycle, but the amplitude is varying in time. Interestingly, for the first cavities, this amplitude modulation is random for the 2D configuration, but is well-correlated for the 3D, suggesting a coherent source of this modulation (Fig. 5, top left). The low frequency associated to this modulation is $1/T_{int} \approx 50Hz - 60Hz$. To further analyze the vortex-noise coupling in acoustic liners, and identify the key frequencies of the oscillations as well as the amplitude modulation, Power Spectral Density (PSD) of the pressure fluctuations at the cavity tips are computed for several locations, namely the cavity n°1, n°21, n°41, n°61, n°81 and n°101. Results are provided in Figs. 7 and 8 for both the 2D and 3D acoustic liners. First, for the 2D configuration, spectra look similar than the one obtained for one single cavity (Fig. 2). In particular, a peak at $782Hz$ is obtained, compared with $743Hz$ for case *C1_3D_U*: this mode corresponds to the quarter wave mode ($m = 1$) inside the cavity, which is given theoretically by:

$$f_m = \frac{(2m-1)c_0}{4(H+\delta H)} \tag{4}$$

where $m \in \mathbb{N}$ is the modal order of the mode, and δH is a correction accounting for 3D effects on the acoustic propagation, which can be approximated by $\delta H = 0.4W_X$ for closed pipes, leading to $f_1 \approx 833Hz$. The modal structure of this mode can be visualized in Fig. 6-a, where the rms normalized values of the pressure fluctuations are displayed for various locations inside the cavity, i.e. for $0 < y/H < 1$, where $y/H = 0$ refers to the junction and $y/H = 1$ to the cavity tip. For all cavities, the modal shape is similar to a quarter-wave mode, given analytically (red dashed line in Fig. 6) by :

$$\hat{p}_{th}\left(\frac{y}{H}\right) = \sin\left(\frac{y\pi}{2H}\right) \tag{5}$$

Additionally, the harmonics of this mode are also observed in the spectra, in particular the first harmonics $m = 2$ at $2514Hz$ associated with the theoretical frequency $f_2 \approx 2500Hz$. It can be noticed that only this fundamental mode and its harmonics can be observed in the spectra, which suggests that the amplitude modulation observed in the 2D case is not locked-in with a fixed frequency. Note also that along the liner, the PSD of the pressure inside the cavity does not vary in term of frequency content: only the level is slightly reduced for cavity located further downstream in the acoustic liner.

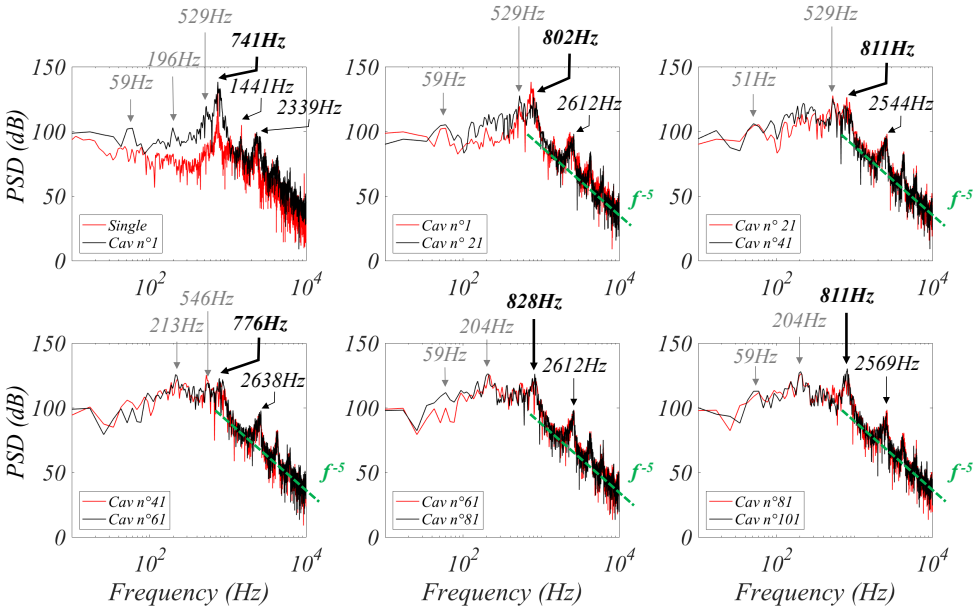

Fig. 8 Power spectral density (PSD) of the fluctuating pressure at six cavity tips (n°1, n°21, n°41, n°61, n°81 and n°101) for the case *C101_3D_U*. The evolution of the spectrum along the liner is highlighted by superimposition of the current spectrum (black) with the previous one (red). For the first cavity, the spectrum is compared with the one from the single-cavity case *C1_3D_U*.

PSD for the 3D unstable configuration exhibits a similar frequency content than the 2D case (Fig. 8), where again the quarter-wave mode and its harmonics can be observed. However, the PSD also exhibits additional frequencies, not observed either in the 2D configuration or in the single-cavity case (they are highlighted in grey in Fig. 8). They corresponds to low-frequency modes appearing at frequency $59Hz$, $204Hz$ and $529Hz$. Interestingly, the amplitude modulation observed in Fig. 5 with a frequency $1/T_int \approx 50Hz - 60Hz$ is clearly retrieved in the spectrum for almost all cavity locations. This is one major difference with the 2D case where an amplitude modulation was also present, but not locked in frequency. Moreover, the PSD for the first cavity exhibits all these low-frequency modes, while the incoming grazed boundary flow does not contain any unsteadyness (no synthetic turbulence is injected at the inlet, so the incoming flow for the first cavity is purely steady). It suggests that this modulation comes from the excitation by the other downstream cavities, and therefore has an acoustic nature. Indeed the hydrodynamic perturbations can only be convected downstream, so that the first cavity cannot interact with downstream cavity through this type of perturbations, whereas acoustic waves can travel upstream at a speed $U_X - c_0 < 0$.

Finally, the correlation between the hydrodynamic perturbations in the shear layer and the acoustic level in the cavity is proposed in Fig. 9, for both the 2D (top) and 3D (bottom) cases. To do so, the y-component of the velocity field V/U_b at the axial cavity location and $y/H = -0.1$ is considered. Its rms value is shown for various cavity locations, from the first to the last cavity. For both cases, a rapid growth of the velocity fluctuations is observed for the first 8 cavities. Then, a different scenario is played depending on the 2D or 3D configuration. In 2-dimension, the velocity fluctuations decrease all along the liner through an exponential decay. However, in 3-dimension, no decay of the fluctuating velocity is noticed: the rms valu is constant for all cavities, so that $V^{sl}_{rms}/U_b \approx 0.075$. The acoustic level at the cavity locations is obtained as the rms value of the pressure oscillations at the cavity tip, i.e. $y/H = 1$. Again, two scenarios are depicted in Fig. 9 (middle). For both cases a strong amplitude is obtained for the first 10 cavities, corresponding to the locations where a rapid growth of the hydrodynamic perturbations was found. Then, for the case *C101_2D_U*, the acoustic level decreasing exponentially, as for the hydrodynamic fluctuations. However, for case *C101_3D_U*, the acoustic level is even increasing linearly with the axial distance, suggesting that the acoustics inside the cavity is not only driven by the hydrodynamic perturbation at the same location (other wise all cavities $N_c > 10$ having the same velocity fluctuation would have the same acoustic level), but potentially by cumulative effects. To further investigates the evolution of the hydrodynamic perturbation with the axial location of the cavities, the PSD of the y-component of the velocity field is carried out for three positions: cavity n°1, n°51 and n°101 (Fig. 9, right). It is shown that for the first cavity, both 2D

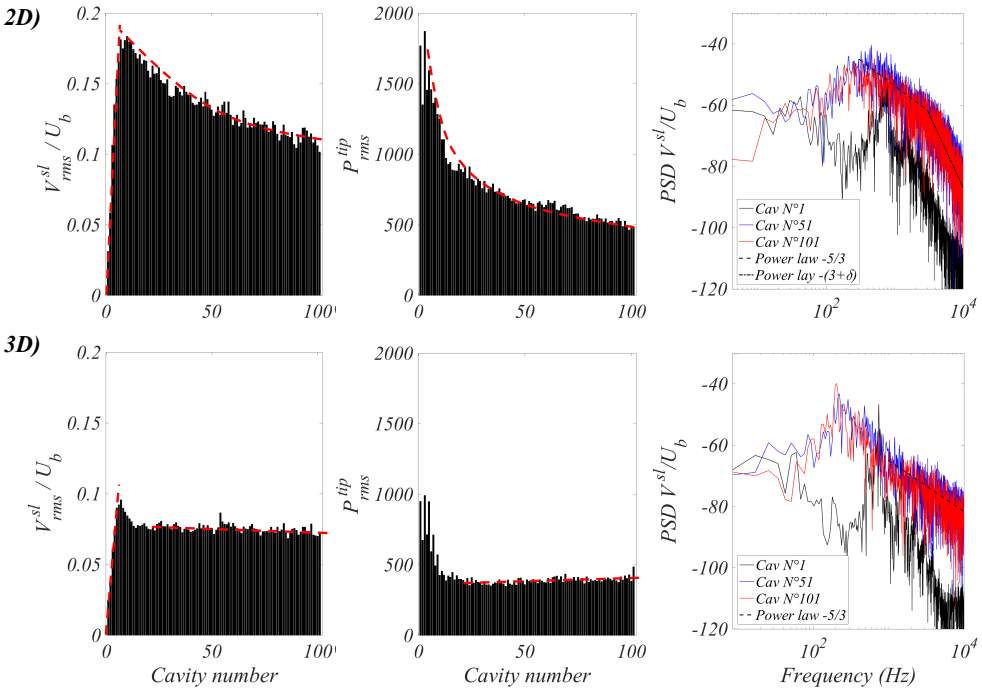

Fig. 9 Rms value of the y-component of the velocity in the shear layer V^{sl}_{rms}/U_b (left), rms value of the pressure at the cavity tips (middle) and PSD of the y-component of the velocity field in the shear layer (right) for both the 2D (top) and 3D (bottom) cases. $\delta \approx 1.8$ is the Boffetta and Musacchio [33] slope correction accounting for viscous effects.

and 3D case lead to a similar spectrum with a large peak at the resonance frequency close to $800Hz$, and a rapid decay of the energy for higher frequencies. Note that for the two configurations, the spectra are not changing significantly after the 51^{st} cavity, a results also obtained for the shape factor that was contant after the 21^{th} cavity, denoting the nature of the boundary layer was no more evolving. For further downstream location however, the PSD spectra are different depending on the 2D or 3D cases. In 2-dimension, a peak is observed at $454Hz$, which is much smaller than the resonance peak close to $750Hz$-$800Hz$. Note that such a peak at a lower frequency was not obtained in the acoustic spectra for the 2D case. For frequencies higher than the peak frequency, two different regimes are obtained, typical of the double cascade encountered in 2D turbulent flows. The first regime corresponds to the energy flux regime characterized by a slope $-5/3$. The second regime is associated with the enstrophy flux, and is characterized by a slope close to -3. Boffetta and Musacchio [33] provide a more detailed analysis of this peculiar regime, concluding that this larger slope can be (i) either due to a lack of resolution of the small flow structures, and/or (ii) a viscous effect (i.e. Reynolds effect), since the slope -3 is obtained for a inviscid flow. For the viscosity ν used in the present simulation, the slope correction proposed by Boffetta and Musacchio [33] is $\delta \approx 1.8$. This value gives a slope $-(3+\delta)$ in good agreement with the present results (**-·-·** in Fig. 9, top right). In 3-dimension, the PSD spectra are different. First, the peak is observed at the resonance peak close to 800Hz. Moreover, the low-frequency modes are visible for all cavities, in particular the first cavity showing a strong peak close to 60Hz. For higher frequencies, the classical Kolmogorov cascade with a slope $-5/3$ is obtained. As a conclusion, these results demonstrates that a trace of the 60Hz mode is visible in the velocity fluctuations inside the shear layer. These perturbations, observed also at the first cavity, could have been excited by acoustic waves coming from the other cavities (since the incoming boundary layer steady in the present case, it cannot contribute to this frequency content).

IV. Conclusion

This present study has investigated numerically the interaction between the hydrodynamic perturbations in the boundary layer and the acoustic waves inside the cavities of an acoustic liner configuration containing 101 cavities.

After the analysis of a single-cavity case revealing a strong vortex-noise coupling at 750Hz, the complete multiple-cavity case was computed both in 2D and 3D. When the acoustic feedback loop is cut off, no vortex-noise coupling at $750Hz$ is observed. However, large flow structures inside the boundary layer emerge. When switching on the acoustic feedback loop by using reflecting boundary conditions, a strong vortex-noise coupling is again present, at the same frequency $750Hz$, for both the 2D and 3D configurations. In the 2D case, no other peculiar modes are observed. However in the 3D case, large hydrodynamic flow structures can be noticed, similar to the ones observed when the acoustic feedback loop was switched off. Low-frequency modes are also obtained in PSD, both on the acoustic pressure oscillations inside the cavity and on the hydrodynamic velocity fluctuations inside the shear layer. It therefore demonstrates the presence of such typical structures, also obtained by LNSE or experiment in the literature. Further work is still required to keep on analyzing the complex competition occuring between the turbulent boundary layer and the acoustic waves inside the multiple cavities, in particular some possible synchronization mechanisms. One possible scenario proposed here is that upstream of the liner, the vortex-noise instability at $750Hz$ is dominated. However, further downstream, the shear layer becomes thicker, thus more stable and robust to transverse acoustic waves, leaving the place for the large flow structures to exist. Large Eddy Simulations of 3D compressible flows have been proved here to be an effective tool to obtained fine details on both ingredients of this coupling: the hydrodynamic instability of the shear layer and the acoustic waves inside the cavities.

References

[1] Pollack, M., "Flow-induced tones in side-branch pipe resonators," *J. Acoust. Soc. Am.*, Vol. 67, No. 4, 1980, pp. 1153–1156.

[2] Ziada, S., and Shine, S., "Strouhal numbers of flow-excited acoustic resonance of closed side branches," *J. Fluids Struct.*, Vol. 13, No. 1, 1999, pp. 127–142.

[3] Geveci, M., Oshkai, P., Rockwell, D., Lin, J.-C., and Pollack, M., "Imaging of the self-excited oscillation of flow past a cavity during generation of a flow tone," *J. Fluids Struct.*, Vol. 18, 2003, pp. 665–694.

[4] Ma, R., Slaboch, P., and Morris, S., "Fluid mechanics of the flow-excited Helmholtz resnator," *J. Fluid Mech.* , Vol. 623, 2009, pp. 1–26.

[5] Graf, H. R., and Ziada, S., "Excitation source of a side-branch shear layer," *J. Sound Vib.* , Vol. 329, 2010, pp. 2825–2842.

[6] Morris, S., "Shear-layer instabilities: Particle Image Velocimetry measurements and implications for acoustics," *Annu. Rev. fluid Mech.*, Vol. 43, 2011, pp. 529–550.

[7] Nakiboglu, G., Manders, H., and Hirschberg, A., "Aeroacoustic power generated by a compact axysymmetric cavity: prediction of self-sustained oscillation and influence of the depth," *J. Fluid Mech.* , Vol. 703, 2012, pp. 163–191.

[8] Gikadi, J., Foller, S., and Sattelmayer, T., "Impact of turbulence on the prediction of linear aeroacoustic interactions: acoustic response of a turbulent shear layer," *J. Sound Vib.* , Vol. 333, 2014, pp. 6548–6559.

[9] Boujo, E., Bauerheim, M., and Noiray, N., "Saturation of a turbulent mixing layer over a cavity: response to harmonic forcing around mean flows," *J. Fluid Mech.* , Vol. 853, 2018, pp. 386–418.

[10] Howe, M., "The influence of mean shear on unsteady aperture flow, with application to acoustical diffraction and self-sustained cavity oscillations," *J. Fluid Mech.* , Vol. 109, 1981, pp. 125–146.

[11] Tonon, D., Willems, J., and Hirschberg, A., "Self-sustained oscillations in pipe systems with multiple deep side branches: prediction and reduction by detuning," *J. Sound Vib.* , Vol. 330, 2011, pp. 5894–5912.

[12] Meyer, E., and Kurtze, G., "Experiments on the influence of flow on sound attenuation in absorbing ducts," *Journal of the Acoustical Society of America*, Vol. 30, No. 3, 1958, pp. 165–174.

[13] Brandes, M., and Ronneberger, D., "Sound amplification in flow ducts lined with a periodic sequence of resonators," *Proceedings of the 1st AIAA/CEAS*, 1995.

[14] Juschke, M., "Akustische beeinflussung einer instabilitat in kanalen mit uberstromten resonatoren," Ph.D. thesis, 2006.

[15] Marx, D., Auregan, Y., Bailliet, H., and Valiere, J.-C., "PIV and LDV evidence of hydrodynamic instability over a liner in a duct with flow," *J. Sound Vib.* , 2010.

[16] Rienstra, S., and Darau, M., "Boundary-layer thickness effects on the hydrodynamic instability along an impedance wall," *J. Fluid Mech.* , Vol. 671, 2011, pp. 559–573.

[17] Marx, D., and Aurégan, Y., "Comparison of experiments with stability analysis predictions in a lined flow duct," *16th AIAA/CEAS Aeroacoustics Conference*, Vol. AIAA-2010-3946, No. 1-17, 2010.

[18] Dai, X., and Aurégan, Y., "A cavity-by-cavity description of the aeroacoustic instability over a liner with a grazing flow," *J. Fluid Mech.* , Vol. 852, 2018, pp. 126–145.

[19] Xin, B., Sun, D., Jing, X., and Sun, X., "Numerical study of acoustic instability in a partly lined flow duct using the full linearized Navier-Stokes equations," *J. Sound Vib.* , Vol. 373, 2016, pp. 132–146.

[20] Burak, M., Billson, M., Eriksson, L.-E., and Baralon, S., "Validation of a time-and-frequency-domain grazing flow acoustic liner model," *AIAA Journal*, Vol. 47, No. 8, 2009, pp. 1941–1848.

[21] Poinsot, T., and Lele, S., "Boundary conditions for direct simulations of compressible viscous flows," *J. Comput. Phys.* , Vol. 101, No. 1, 1992, pp. 104–129. https://doi.org/10.1016/0021-9991(92)90046-2.

[22] Tam, C., and Auriault, L., "Time domain impedance boundary conditions for computational aeroacoustics," *AIAA Journal*, Vol. 34, No. 5, 1996, pp. 917–923.

[23] Scalo, C., Bodart, J., and Lele, S., "Compressible turbulent channel flow with impedance boundary conditions," *Physics of Fluids*, Vol. 27, No. 1-24, 2015.

[24] Bodart, J., Shelekhov, G., Scalo, C., and Joly, L., "Separation delay via hydro-acoustic control of a NACA 4412 airfoil in pre-stalled conditions," *55th AIAA Aerospace Sciences Meeting*, 2017.

[25] Zhang, Q., and Bodony, D., "Numerical investigation of a honeycomb liner grazed by laminar and turbulent boundary layers," *J. Fluid Mech.* , Vol. 792, 2016, pp. 936–980.

[26] Shelekhov, G., Bodart, J., and Joly, L., "Simulation of the resonant interactions between a boundary layer and an array of deep cavities," *Proceesings of the TSFP conference*, 2017, pp. 1–6.

[27] Vreman, A. W., "An eddy-viscosity subgrid-scale model for turbulent shear flow: algebraic theory and applications," *Phys. Fluids* , Vol. 16, No. 10, 2004, pp. 3670–3681.

[28] Rockwell, D., and Naudascher, E., "Review: self-sustaining oscillations of flow past cavities," *Trans. ASME. J. Fluids Eng.* , Vol. 100, 1978, pp. 152–165.

[29] Bermejo-Moreno, I., Campo, L., Larsson, J., Bodart, J., Helmer, D., and Eaton, J. K., "Confinement effects in shock wave/turbulent boundary layer interactions through wall-modelled large-eddy simulations," *J. Fluid Mech.* , Vol. 758, 2014, pp. 5–62.

[30] Ham, F., Mattsson, K., Iaccarino, G., and Moin, P., "Towards time-stable and accurate LES on unstructured grids," *Lecture Notes in Computational Science Engineering*, Vol. 56, 2007, pp. 235–249.

[31] Bermejo-Moreno, I., Bodart, J., Larsson, J., and Barney, B., "Solving the compressible Navier-Stokes equations on up to 1.97 millon cores and 4.1 trillion grid points," *IEEE International Conference on High Performance Computing*, 2013.

[32] Bauerheim, M., Boujo, E., and Noiray, N., "Numerical analysis of the linear and nonlinear vortex-sound interaction in a T-junction," *AIAA/CEAS Aviation Forum and Exposition*, 2020.

[33] Boffetta, G., and Musacchio, S., "Evidence for the double cascade scenario in two-dimensional turbulence," *Physical Review E*, Vol. 82, No. 016307, 2010.